Safety of high-speed train passing by windbreak breach with different sizes

Sun, Zhuang; Dai, Huanyun; Hemida, Hassan; Li, Tian; Huang, Caihong

DOI:
10.1080/00423114.2019.1657909

Safety of High-Speed Train Passing by Windbreak Breach with Different Sizes

Zhuang Sun[a,b], Huanyun Dai[a*], Hassan Hemida[b], Tian Li[a], Caihong Huang[a]
a State Key Laboratory of Traction Power, Southwest Jiaotong University, Chengdu 610031, Sichuan, People's Republic of China;
b School of Engineering, University of Birmingham, Edgbaston, Birmingham, B15 2TT, United Kingdom.
Email: sunzhuang802@163.com

The safety of a high-speed train running at a speed of 120km/h is investigated when the train passes by windbreak breach with variety of lengths subjected to normal wind speed of 32m/s. Eight lengths of breach are investigated; 50, 35, 25, 15, 12, 10, 7 and 2m. The transient aerodynamic loads of the high-speed train are calculated using the Unsteady Reynolds-averaged Navier-Stokes (URANS) model. The simulation results are validated using field test data on the breach of 12m length. The results showed that although the short windbreak breach produces the highest wind speed it gives the lowest wind loads compared to the longer breach. The train derails when passing by the breaches with lengths 50 and 35m. When the breach length is between 12m and 35m, the first wheelset on the windward side tends to climb up the rail. When the breach length is less than 10m, the derailment coefficient is below 0.8. The first wheelset is the most vulnerable wheelset among the four wheelsets as the train passes by the breaches. It has also been found that only when the wheel raise on the derailment side is higher than flange height the wheelset derails out of the rail.

KEYWORDS: crosswind; windbreak breach, derailment; wheel raise, multi-body simulations

1. Introduction

Many new phenomena and problems are gradually emerged with the rapid development of high-speed railway. China is a vast country with a complex geographical environment and variable climate, which leads to the fatal effect of crosswind on the safety of trains. It is a typical safety problem for trains to operate under the strong crosswind on Lanzhou-Xinjiang line in west of China. The Lanzhou-Xinjiang line was built in the vast desert in which there are many windy zones, which requires windbreak walls built to protect trains. However, in order to rebuilt or optimize the windbreak wall structure, the windbreaks are sometimes opened. It is, however, very dangerous when trains pass by those gaps under crosswind as the high velocity wind passing in these gaps poses a safety risk to the train safety. Field tests were carried out to measure the wheel-rail forces of high-speed train on Lanzhou-Xinjiang line. The wind speed estimated was more than 20 m/s [1]. A very interesting phenomenon was found as the derailment coefficient of first wheelset on the windward side reaches the maximum allowable value 0.8 when the train passes by the breach. The derailment coefficient is based on the 'Nadal formula'. The left and right lateral wheel-rail forces are in the opposite direction, while

the left and right vertical wheel-rail forces are loading and unloading, respectively. The left side of the wheelset is the leeward side and the right side of the wheelset is the windward side. Usually the derailment coefficient of wheel on the leeward side becomes higher than that of wheel on the windward side since the wheelset is forced to move to the leeward side by crosswind. In order to analyse this interesting phenomenon, vehicle multibody dynamics model and aerodynamics model were built. Sun et al. [2] reproduced the tested phenomenon by simulation method when the train passes by the 12m breach. It was an unplanned field test that the accurate wind speed was not collected near the windbreak wall. According to the weather forecast, the wind speed was almost 32 m/s. Therefore, as long as wind loads can be obtained to reproduce this phenomenon with the derailment coefficient around 0.8, both the CFD and train dynamics models are considered acceptable. Based on the similar derailment coefficient with the 12 m breach, the effect of the gap size can be included in this investigation.

Some researchers have studied some dynamic responses and flow structures of trains when the trains run through complex terrain and climatic conditions. Wang et al. [3] studied the aerodynamic characteristics of EMU train passing by windbreak wall gap under crosswind. The surface pressure and the aerodynamic forces of train were analysed. Nevertheless, the pitch moment and yaw moment of the train have not been calculated. In addition, the simulation model has not been validated by field test or wind tunnel experiment. Liu et al. [4, 5] measured and studied the car-body lateral vibration response of high-speed train negotiating complex terrain sections under strong crosswind. A new train motion phenomenon named ‘carswaying’ has been found in field test. Liu et al. [6] analysed the flow structure around a high-speed train passing by a windbreak transition under crosswind and calculated the critical wind speed based on the EN14067-6. Li et al. [7] studied dynamic performance of high-speed train passing by windbreak in crosswind and optimized the windbreak structure. Miao et al. [8, 9] studied the aerodynamic characteristic of train on the bridge built between two mountains. It has been found that the wind is speeded up in the middle of vale with the width of the vale decreasing. Li et al. [10] analysed the flow around a high-speed train moving through a gust zone. A kind of gust wind was simulated by changing the inlet velocity value. Baker et al. [11, 12, 13, 14] reviewed a research framework of crosswinds on trains and proposed a new method to calculate unsteady wind loadings acting on a railway vehicle. Hemida et al. [15, 16, 17, 18] studied the flow structure around trains and frequency of aerodynamic forces based on the large-eddy simulation (LES). Howell [19] found that the duration and magnitude of experimental yaw moment coefficient became extended with a longer gust zone when the train passed through a crosswind gust zone in the laboratory. Kohama et al. [20] found the peak of yaw moment was caused by negative pressure resulting from a vortex occurring on the lee side. However, those researchers have not to pay attention to the train safety when the train passes by the windbreak breaches.

As field tests under crosswind is very dangerous and unrepeatable, the flow structure and safety of the train are predicted in this paper using the validated vehicle multibody dynamics model and aerodynamics model. The only modified parameter in this study is the breach length and eight breaches with different lengths were investigated; 50m, 35m, 25m, 15m, 12m, 10m, 7m and 2m. The field test is described in Section 2. In Section 3, a simplified vehicle model and eight flow field domains including the windbreaks and different length breaches are described in detail. The mesh around the windbreak and train surface are shown. The y+ around the train surface and grid independence are described. The transient aerodynamic forces and moments were calculated using the Fluent software package [21], and acted on the vehicle dynamic model. In addition, the suspension parameters and the mass as well as

rotary inertia of each part of train are described in detail in this section. The vehicle dynamic train model was constructed by the multi-body simulation software SIMPACK [22]. In Section 4, velocity and pressure field around the train are analysed when the train passes by windbreak breach with different sizes. The responses of the train are analysed in detail in Section 5, where five indexes are analysed. These are the derailment coefficient, overturning factor, wheel raise, lateral distance and yaw angle of the first wheelset. The trend of wheel climbing up rail with the breach length changing is analysed in detail. Conclusions are presented in Section 6.

2. Field tests

The field test was carried out in Baili windy zone on the Lanzhou-Xinjiang line under strong crosswind with the wind speed about 20-32m/s. The Baili windy zone is shown in Figure 1.(c). The total length of the Lanzhou-Xinjiang line is 1776km, which is built in four windy zones; Anxi windy zone, Yandun windy zone, Baili windy zone and Dabancheng windy zone. The total length of those windy zones is about 579.599km [23]. Windbreak walls and Anti-wind Tunnels were built to protect the high-speed trains.

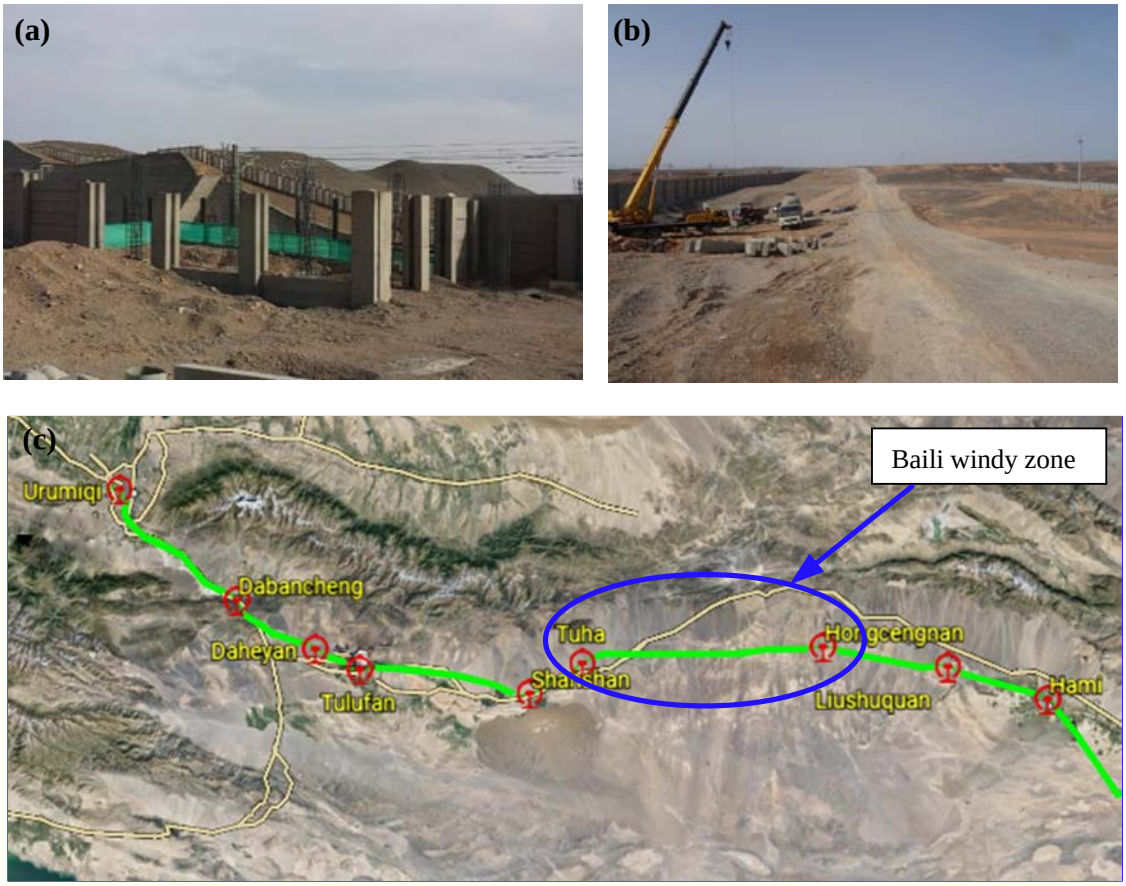

Figure 1 Test environment. (a) Windbreak breach. (b) Terrain outside windbreak. (c) Test area (Lanzhou-Xinjiang line)

windbreak are shown in Figure 1.(a) and 1.(b), respectively. The map of the Lanzhou-Xinjiang line is shown in Figure 1.(c).

Correspondingly, a very interesting phenomenon was measured and it was found that the derailment coefficient of the first wheelset on the windward side reached the allowable value of 0.8. Meanwhile, the left and right lateral wheel-rail forces were in the opposite direction. There was only the first wheelset that collected the wheel-rail force, the others wheelsets of the first car were common wheelset. According to the GB5599-85, the derailment coefficient must not exceed the limited value 0.8. The instrumented wheelset with some strain gauges constituting the Wheatstone bridge was applied to collect the wheel-rail force as shown in Figure 2 (a). All settings about the instrumented wheelset could be found in the standard of GB5599-85 [27]. The vehicle speed was monitored by the vehicle speed sensor (VSS) shown in Figure 2 (b), which could be used for the CFD simulation in Section 3. After the train passing by the breach, the train started to brake for safety.

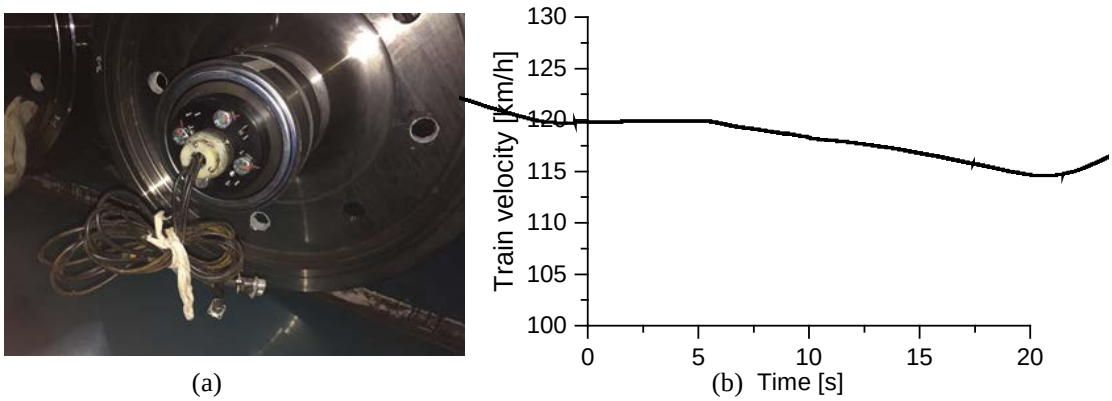

(a) (b)

Figure 2 (a) Instrumented wheelset, (b) Train velocity

3. Simulation Model

3.1 Aerodynamic model

In order to reproduce the aerodynamic forces and moments acting on the train when passing by the breaches, the computational fluid dynamics (CFD) method was used. The aerodynamic model, in which the windbreak, breach, and terrain were simplified is shown in Figure 3. The rugged terrain was simplified to a plain, and the height of windbreaks was the uniform value of 3 m. The windbreaks were not rising and falling with the terrain. The section of the breach was simplified to a rectangle ignoring obstacles, and the bogies of the train were ignored. Due to trade secrets, the specific model name of the train cannot be provided. Sun et al. [2] have validated the aerodynamic model and the multibody dynamic model by comparing the grid independence and the tested rail-wheel force when the train passes by the 12 m breach.

The crosswind entered the domain with a uniform velocity of 32m/s. A zero pressure boundary condition was implemented at the domain exit. A symmetry boundary condition was set for the top of domain. No-slip boundary conditions were used on the ground and the train surface. The sliding mesh technique was used to simulate the movement of the train in which there were two sub domains; a moving domain containing the train, and a stationary domain containing the windbreak wall and breach.

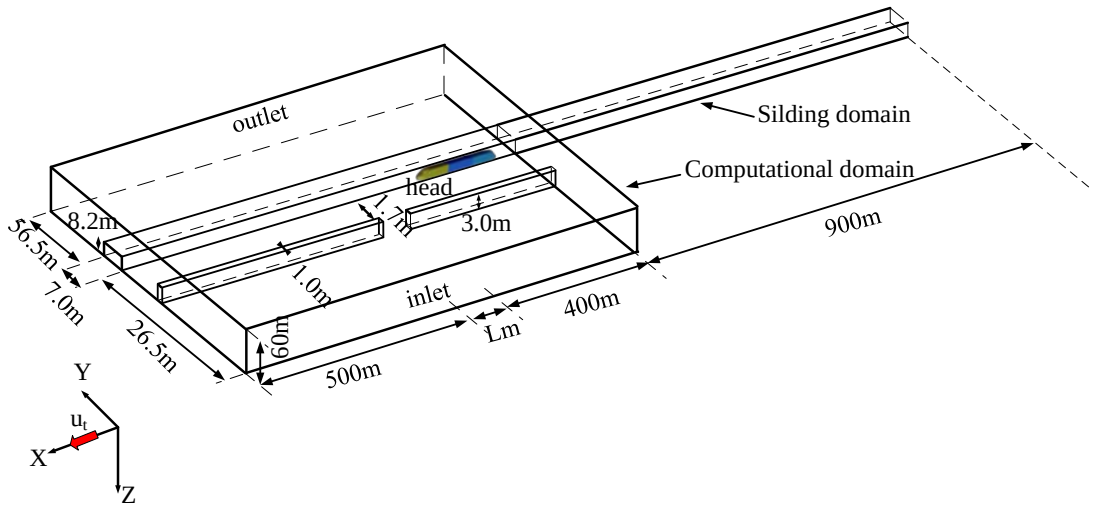

Figure 3 Generalised domain.

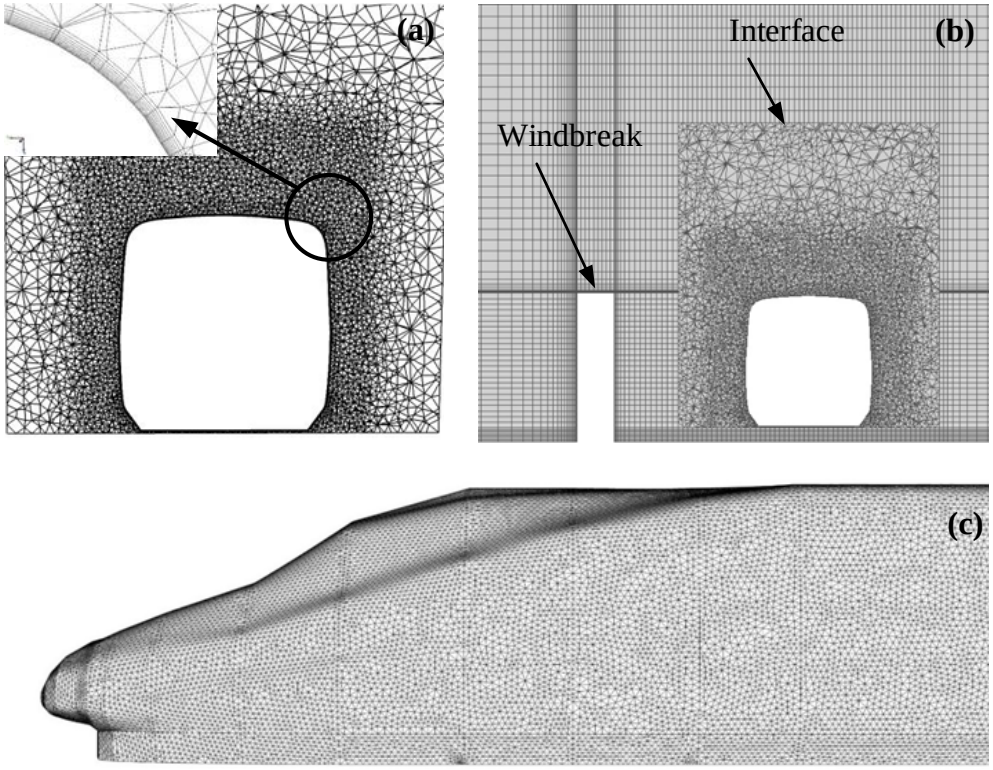

Figure 4 Computational Mesh 5 :(a) boundary layer (b) domain mesh (c) mesh around the train surface

The Semi-Implicit Method for Pressure-Linked Equations (SIMPLE) algorithm used for the pressure-velocity coupling. The realizable k-ε turbulence model with standard wall function was adopted to calculate the flow felid. This turbulence model and standard wall function were successfully used by Sima, Kang and Chen et al. [24,25,26] to solve for the flow around high-speed trains and cars. The gradients are computed in ANSYS Fluent according to the least squares cell-based. The second order discretization scheme is available for the pressure equation. Second-order upwind convection-diffusion equations were used in all the considered cases. The residuals of continuity, velocity, kinetic energy, and epsilon are below 8.0542e-4, 6.6283e-06, 3.9536e-05 and 5.59511e-05, respectively. The eight cases of breaches lengths were simulated using the Fluent software on the high-performance computational platform of the Southwest Jiaotong University. The time step used in

the simulation was set to be 0.001 s and simulation duration time was 10 s. A typical simulations takes about 6 days for calculating each case on 128 processors.

Five sets of meshes were created to analysis mesh sensitivity based on the changing of aerodynamic forces. The number of cells of Mesh1, Mesh2, Mesh3, Mesh4, and Mesh5 was 2.58 million, 5.83 million, 9.06 million, 13.01 million and 26.87 million, respectively. The boundary layer height was 1.0 mm. The out domain is filled with the structure hexahedral mesh and the sliding domain is filled with tetrahedral mesh. The side force tended to converge from Mesh 4 to Mesh 5, while in the paper the Mesh 5 was calculated because the flow field could be smoother near the sliding interface. Meanwhile, the accuracy of the wind loads for the train dynamic is accepted. The y+ near the train surface is shown in Figure 5. When the train passes by the breach, the maximum y+ is about 120 on the windward surface. The y+ of two section curves around the train surface are shown in Figure 5. The initial points are the grey points on the train surface. For the realizable k-ε turbulence model with standard wall functions, the y+ is accepted.

Table 1 Mesh independence data

Mesh	Cells (million)	First height	Number of boundary layer	Side force (kN)
Mesh1	2.58	1mm	10	41.08
Mesh2	5.83	1mm	10	47.78
Mesh3	9.06	1mm	10	51.68
Mesh4	13.01	1mm	10	48.59
Mesh5	26.87	1mm	10	47.33

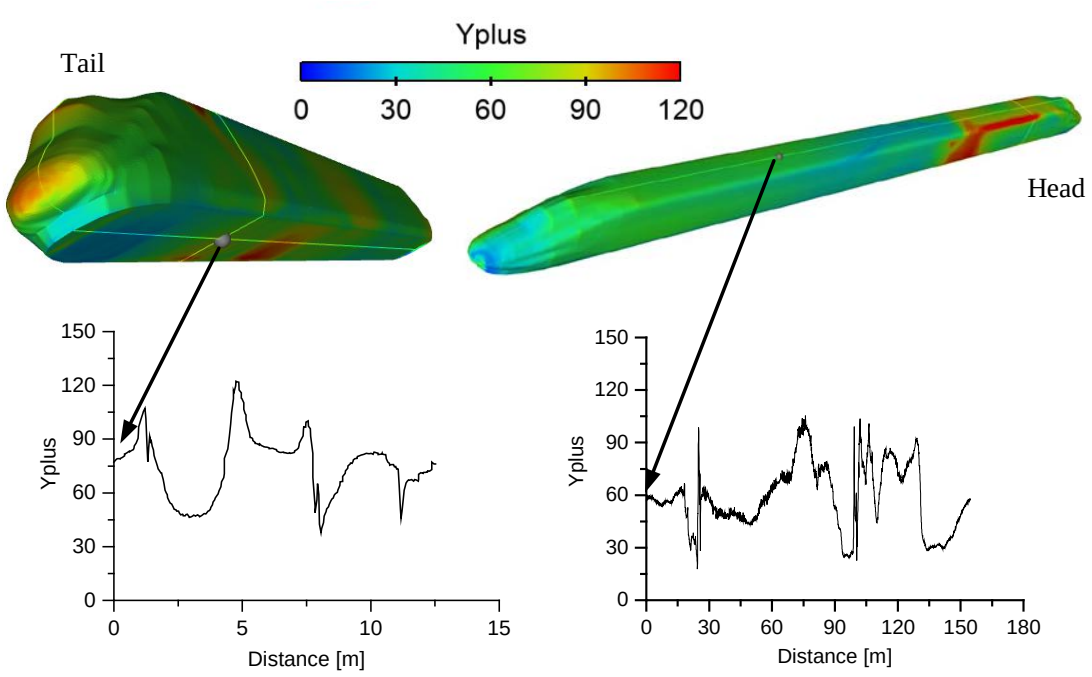

Figure 5 Y+ around the train surface

3.2 Vehicle dynamic model

A full-scale vehicle model was developed by the multi-body simulation software SIMPACK [22]. The vehicle model is a nonlinear dynamic model, including the wheel-rail contact model, elastic stops and nonlinear suspensions. All bodies of the train were assumed rigid, including carbody, bogies,

wheelsets and axle boxes. The track was considered straight but including measured irregularities. The integral time and vehicle speed were 15s and 120km/h, respectively. The frequency of output was set at 100 Hz.

Table 2 Mass and suspension parameters

parameters	Value	Unit
Mass of carbody	39500	kg
Roll rotary inertia of carbody	61000	$kg \cdot m^2$
Pitch rotary inertia of carbody	1835000	$kg \cdot m^2$
Yaw rotary inertia of carbody	1816000	$kg \cdot m^2$
Mass of frame	2758	kg
Roll rotary inertia of frame	1962	$kg \cdot m^2$
Pitch rotary inertia of frame	2180	$kg \cdot m^2$
Yaw rotary inertia of frame	4003	$kg \cdot m^2$
Mass of wheelset	1721	kg
Roll rotary inertia of wheelset	911	$kg \cdot m^2$
Pitch rotary inertia of wheelset	100	$kg \cdot m^2$
Yaw rotary inertia of wheelset	911	$kg \cdot m^2$
Longitudinal stiffness of air spring	0.18	MN/m
Lateral stiffness of air spring	0.18	MN/m
Vertical stiffness of air spring	0.3	MN/m
Longitudinal stiffness of primary spring (each axlebox)	0.14	MN/m
Lateral stiffness of primary spring (each axlebox)	0.14	MN/m
Vertical stiffness of primary spring (each axlebox)	0.5053	MN/m
Joint stiffness of primary damper	2.5	MN/m
Joint stiffness of secondary damper	3.0	MN/m

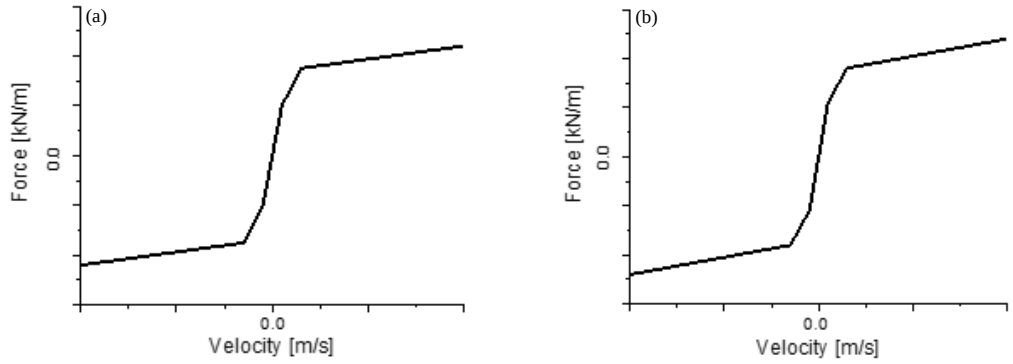

Figure 6 Damping force. (a) Vertical damping of primary damper. (b) Lateral damping of secondary damper

Some key parameter of the mass and suspension parameters are shown in the Table 2. The trends of damping curves are shown in Figure 6. Vertical damping force of primary damper is shown in Figure 6 (a), and Lateral damping force of secondary damper is shown in Figure 6 (b). Usually, the damper should be fixed with joint stiffness. The damper and spring are abstracted and described as type NO. 6 and NO.5 force elements in SIMPACK software. These nonlinear numbers should be put into the Input function model in SIMPACK software.

3.3 Aerodynamic loads

Aerodynamic loads showed the simulation results of the aerodynamic model shown in Figure 7 and Figure 8. With the breach length becoming longer, the wind forces and moments become stronger. Meanwhile, the duration of the wind loads become longer. After the train passing by the breaches, the forces and moments will decrease dramatically.

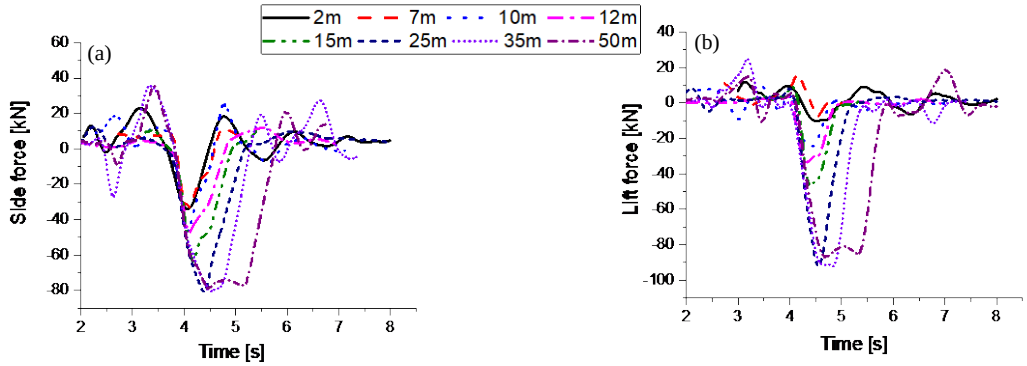

Figure 7 Wind forces. (a) Side force. (b) Lift force

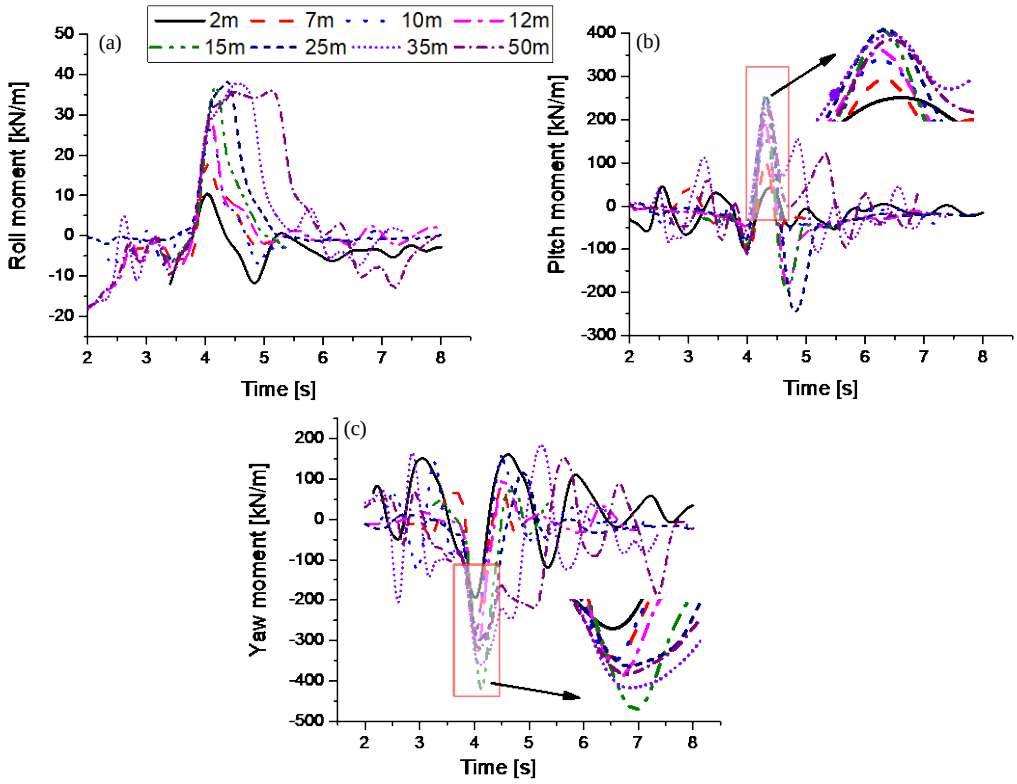

Figure 8 Wind moments. (a) Roll moment. (b) Pitch moment. (c) Yaw moment

The peak values of the side forces are almost equal in magnitude when the breach length is more than 25m. The side forces and lift forces are shown in Figure 7 (a) and (b). After reaching the peak value, the side force of the train decreases gently when the train passes by the breach of 50m from 4.5s to 5s. The same trend can be found on the lift force and roll moment as both decrease gently when passing the breach of 50m. The fluctuation of lift forces at the breach of 2m and 7m is not higher than that of lift forces at others breach. The roll moment, pitch moment and yaw moment are shown in Figure 8. The maximum value of the pitch moment occurs with the train passing by the breach of 15m. These wind forces and moments were acted on the centre of carbody with SIMPACK software. The

safety of the train can be analysed under these crosswinds. The peak values of the pitch and yaw moment of each breach are listed in the Table 3. The train is under the maximum pitch and yaw moment when passes by the 15m. However, the results are determined by the duration and wind loads.

Table 3 The maximum pitch and yaw moment (kN/m)

	2m	7m	10m	12m	15m	25m	35m	50m
Pitch moment	99.91	112.12	159.75	188.82	253.34	252.03	236.39	221.37
Yaw moment	193.92	281.22	286.54	325.70	422.01	298.99	359.78	321.42

4. Flow structure

4.1 Velocity distribution

In order to analyse the flow speed at the breach, velocity contours were plotted on a horizontal plane at 1.8m above the ground and the results are shown in Figure 9.

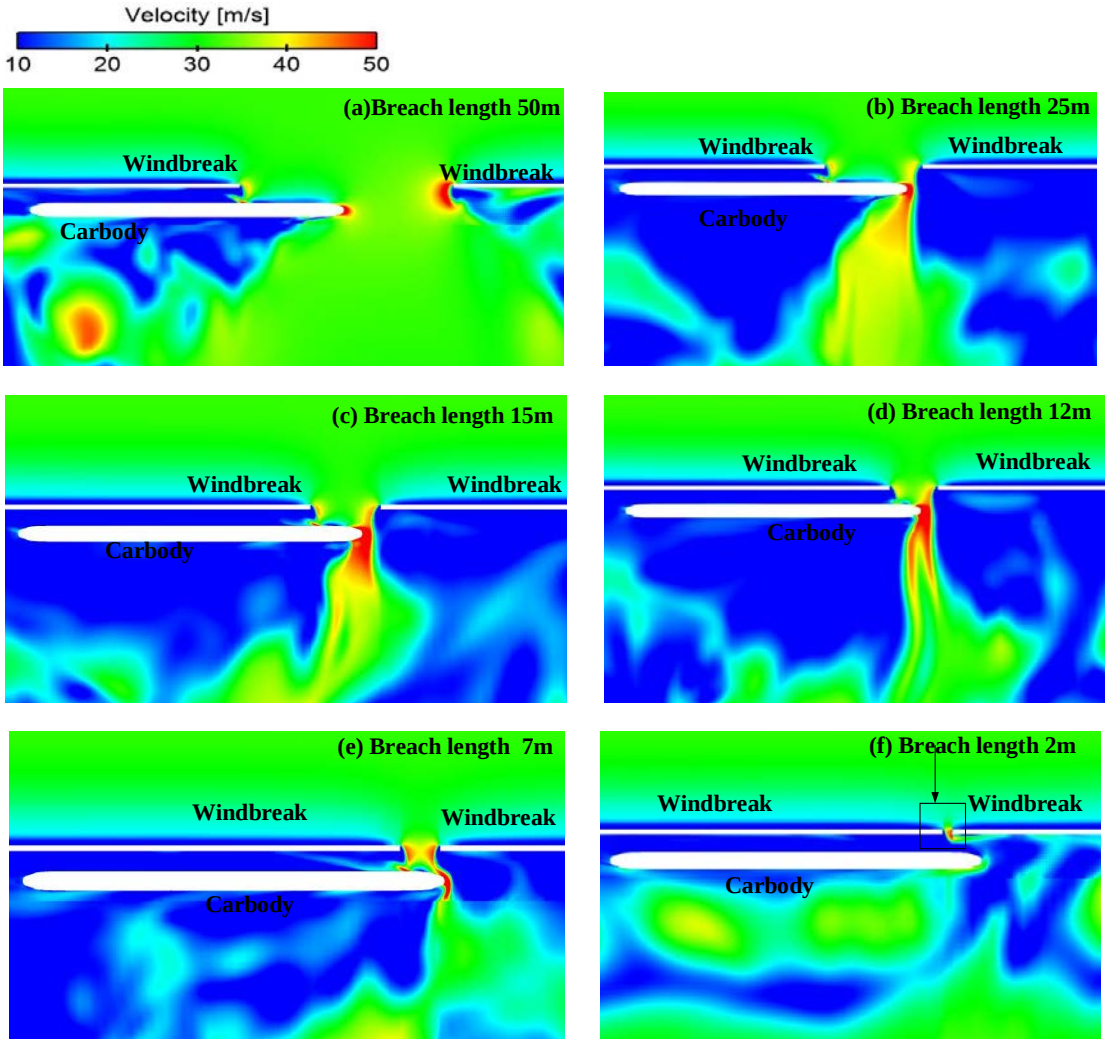

Figure 9 Velocity distribution

This height 1.8m is equal to the height of the centre of gravity of the carbody. It can be seen in Figure 9 that when the breach length becoming shorter, the wind flow speeds up to pass through the

breach. When the breach length is 50m, the flow speed at the breach is equal to inlet velocity as shown in Figure 9 (a). There is slight flow speeding at the edges of the breach. When the breach length is 25m, the main flow speed is equal to or greater than 35m/s as shown in Figure 9 (b). The main flow accelerates to 40-45m/s when the breach length is 15m and 12m as shown in Figure 9 (c) and (d). The maximum value of speed is about 50m/s at the 12m breach as shown in Figure 9 (d). In addition, when the breach length is 7m and 2m, the flow speed is equal to 45-55m/s as shown in Figure 9 (e) and (f).

4.2 Pressure distribution

The peak values of the aerodynamic forces on the train are found when the train passes by the windbreak breach as shown in Figure 7 and Figure 8. In order to analyse the pressure and flow structure around the train, the pressure contours were plotted at near 4.5s on a horizontal plane at 1.8m above the ground and the results are shown in Figure 10. At near 4.5s, the side forces reach the maximum.

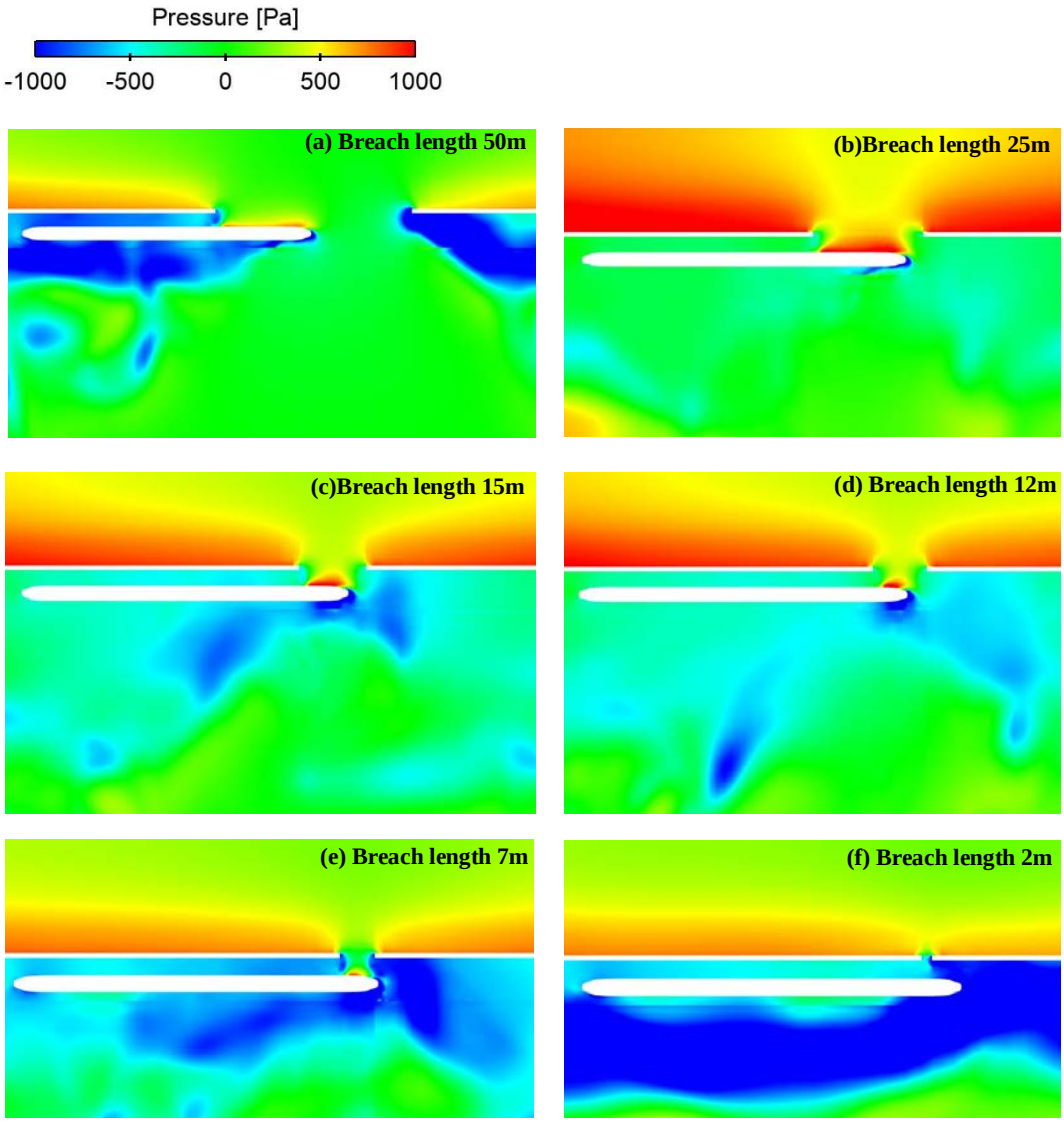

Figure 10 Pressure and flow distribution with train

In Figure 10 (a), the pressure of the head carbody on the windward side is approximately in the range of 500-800 Pa. when the train is at the 25m, 15m and 12m breach, the pressure of the head carbody on

the windward side is in the range of 800-1000 Pa. However, the pressure on the windward side of the carbody decreases to the range of 500-800Pa and the range of 0-500 Pa with the train passing by the 7m and 2m breach, respectively. There is a negative pressure region on the leeward side of carbody at all the breaches. The overall wind forces and moments are shown in Figure 7 and Figure 8. The reason why the changing on pressure is not consistent with the changing on wind loads is that the windward area of the carbody and duration of the gust wind are different as passing by different breaches.

5. Safety analysis

5.1 Derailment coefficient

5.1.1 Derailment coefficient of the first wheel

All the derailment coefficients of the first right wheel passing by different breaches are shown in Figure 11 (a). Low-pass filtering of derailment coefficient with a 40-Hz fourth-order Butterworth filter or another filter is shown to be equivalent [27].

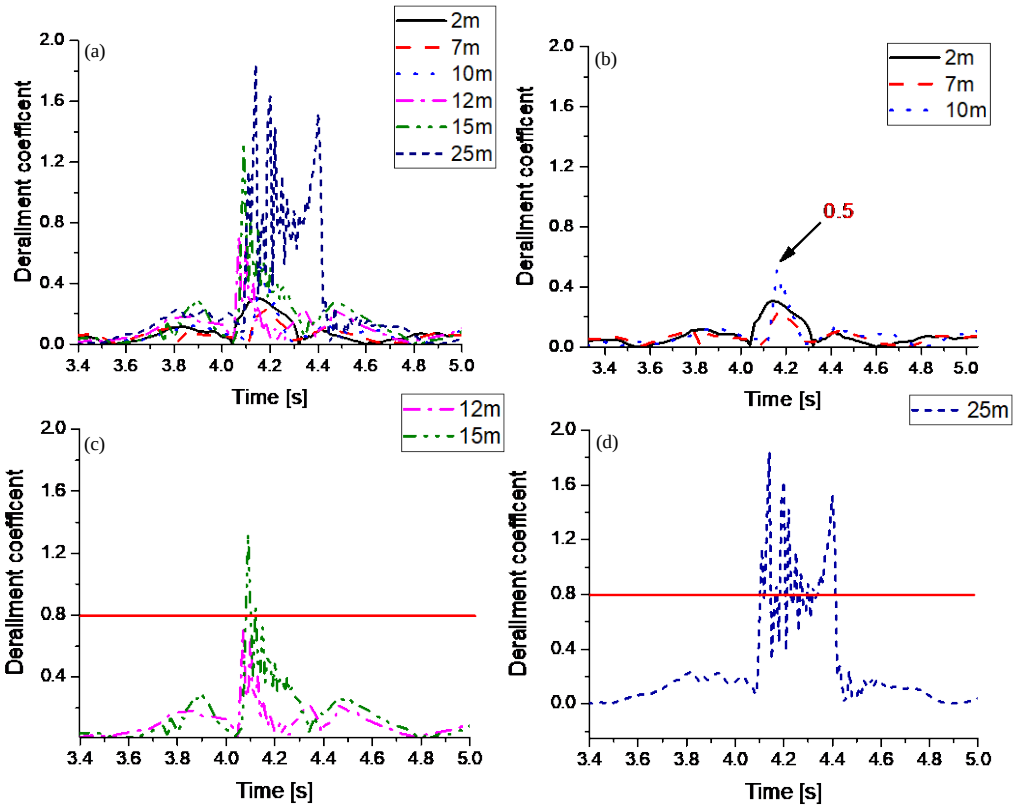

Figure 11 Derailment coefficient of the first right wheel. (a) Total derailment coefficients. (b) Derailment coefficients below the limit. (c) Derailment coefficients above the limit. (d) shows the derailment coefficients when the train passes the 25m breach

Figure 11 (b) shows the derailment coefficients of the first right wheel passing by 2m, 7m and 10m breach. The maximum value is 0.5 when the train passes by the 10m breach. Figure 11 (c) shows the

derailment coefficients of the first right wheel passing by breaches of 12m and 15m. The maximum value of the two lines reaches and exceeds the allowable value of 0.8. Meanwhile, the right wheel flange touches the rail. Figure 11 (d) shows the derailment coefficients of the first right wheel passing by the 25m breach. Although the maximum values of the derailment coefficients exceed the allowable value of 0.8, the wheelset does not derail out of the rail.

The derailment coefficients are not shown when the train passes by the breaches of 35m and 50m because it makes no sense at this moment. The derailment phenomenon could be obtained as analysing the wheel raise and lateral distance of the first wheel in Section 5.3 and Section 5.4.

5.1.2 Derailment coefficient of the 2nd-4th wheelset

The derailment coefficients of the right wheels of the 2nd-4th wheelset are shown in Figure 12. The derailment coefficients of the 2nd-4th wheelset increased, and the peak values do not reach the allowable value of 0.8, except when the train passes by the breach of 12m and 25m.

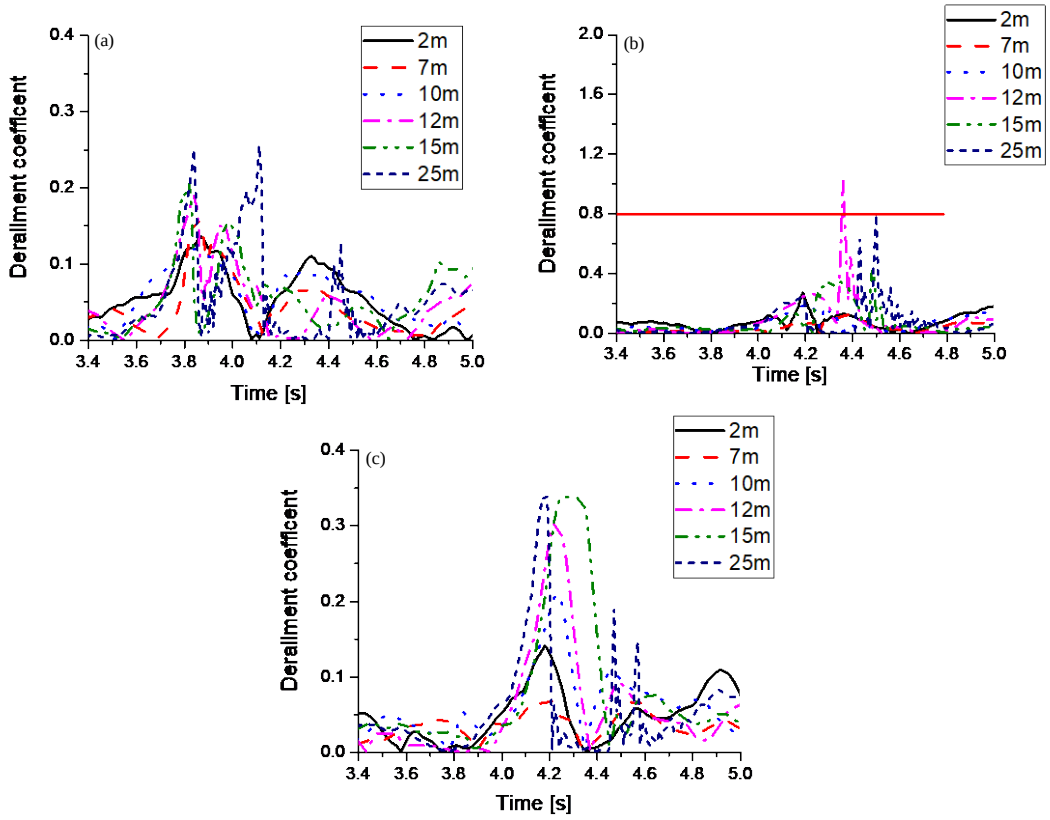

Figure 12 Derailment coefficient of the right wheels. (a) Second wheelset. (b)Third wheelset.(c) Fourth wheelset.

In a very short time, the first wheelset derails out of the rail with dramatically high derailment coefficients when it passes by the breach of 35m and 50m. It doesn't make any sense to display the derailment coefficients when the train has derailed. In order to describe the derailment process, the wheel raise is introduced in Section 5.3. The first and third wheelset is much dangerous than the second and fourth wheelset, and the first wheelset is the most dangerous wheelset among these four wheelsets. Therefore, the safety of the first wheelset should be paid more attention.

5.2 Overturning factor

The overturning factors of the first bogie and second bogie are shown in Figure 13. ΔQ is the unloading of the most critical running gear (bogie or single axle in case of single axle running gear). This unloading shall not exceed 90% of the average static wheel loads [28], Q is the static wheel load.

$$\frac{\Delta Q}{Q} < 0.9 \quad (1)$$

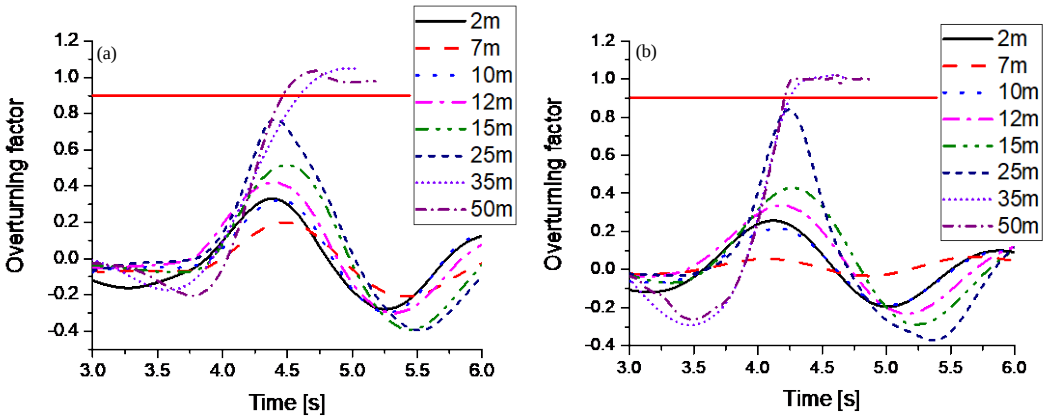

Figure 13 Overturning factor. (a) The first bogie. (b) The second bogie.

It can be seen when the breach length is shorter than 25m, the overturning factors could not reach the allowable value of 0.9. However, when the train passes by the breach longer than the 35m, the overturning factors reach the value of 1.0. There is the same trend for the first and second bogie about the overturning factor. Comparing with the threshold value of the derailment coefficient, the assessment of critical derailment coefficient of 0.8 is much stricter than that of the critical overturning factor as the train passing by breach under crosswind.

5.3 Wheel raise of the first wheel

Wheel raise of the first right wheel and wheel profile are shown in Figure 14, respectively, which is shown that the wheel raise is higher than the height of flange when passing by breaches of 35m and 50m.

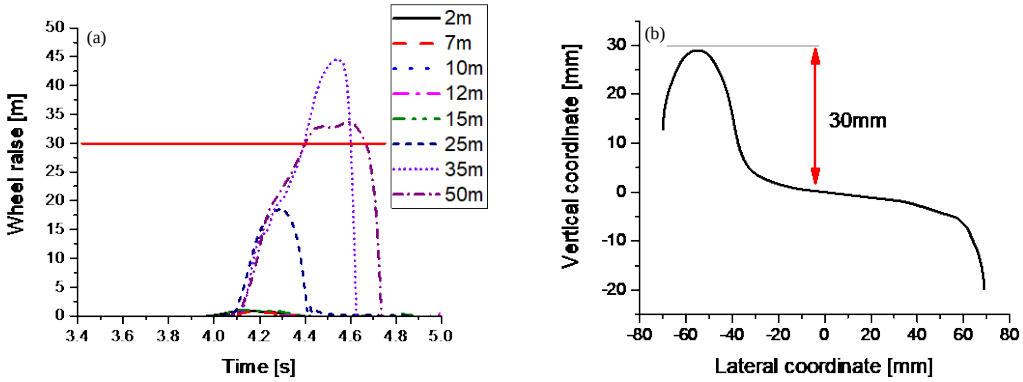

Figure 14 Wheel raise. (a) Wheel raise of the first wheel. (b) wheel profile.

After reaching the peak, the lines of wheel raise to decrease dramatically as passing the breaches of

35m and 55m. This means that the wheel derails out of the rail. Therefore, it is necessary to analyse the wheel raise when studying the derailment. Only when the wheel raise on the derailment side is higher than flange height, the wheelset can derail out of the rail.

5.4 Lateral distance of the first wheelset

Lateral distance of the first right wheel and rail profile are shown in Figure 15. The maximum lateral distance is less than 20mm when the breach length is shorter than 25m. However, the maximum lateral distance is longer than the half width of the rail profile as passing by breaches of 35m and 50m. Figure 16 shows transient images of the right and left wheel when the wheel is climbing up the rail. Figure 16 (b) shows the right flange is climbing up the rail, and Figure 16 (a) shows that the left wheel is falling off the rail.

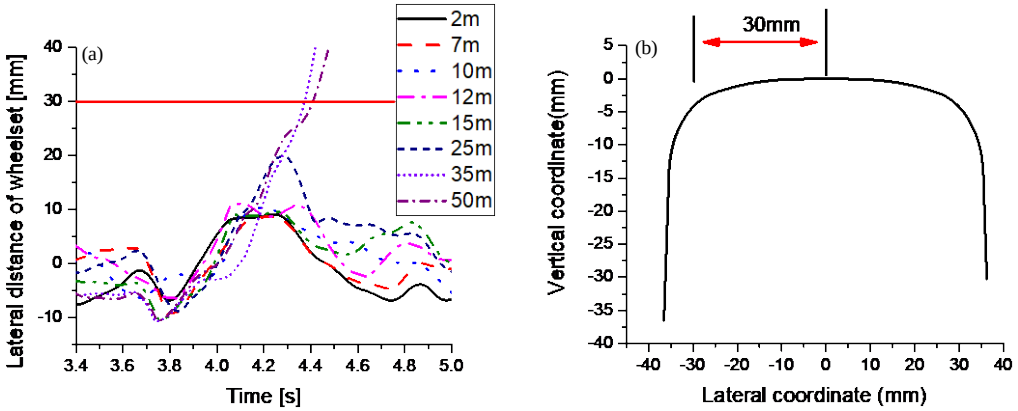

Figure 15 Lateral distance. (a) Lateral distance of the first wheelset. (b) Rail profile.

This is just a transient picture when the wheelset is running out of rail. After climbing up the top of rail, the wheelset will fall off the rail.

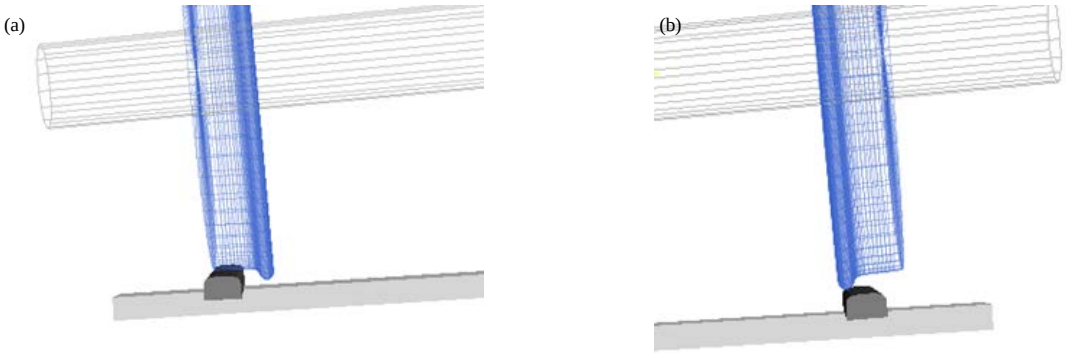

Figure 16 Wheelset: (a) Left wheel. (b) Right wheel

5.5 Yaw angle of the first wheelset

Yaw angle of the first wheelset become lager with the increase of breach's length, which is represented in Figure 17 (a). There is a slight difference in the yaw angle when the train does not derail

passing by the breach shorter than 25m as shown in Figure 17 (b). Only when the wheelset derails out of the rail, the yaw angle becomes larger. It means the lateral motion of the wheelset plays a key role in the derailment rather than the yaw motion of the wheelset.

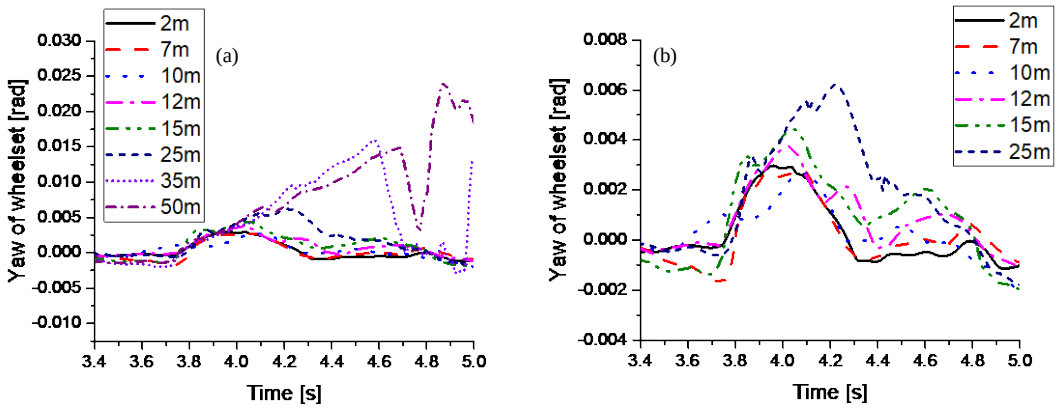

Figure 17 Yaw angle of the first wheelset. (a) Total yaw angles of the wheelset. (b) Yaw angles of non-derailed wheelset

6. Conclusion

The wind loads and flow structure were calculated when the high-speed train passed by different sizes of breach under crosswind. Moreover, the safety of the high-speed train was analysed under those wind loads using SIMPACK software. A typical derailment phenomenon under crosswind is obtained, which includes:

1, The first and third wheelset tends to climb up the windward side rail when the train passes by the different sizes of the breach under crosswind.

2, When the length of the breach is shorter than 35m, the train could pass by the breach safely, however, when the breach's length is longer than 35m, the train derails out of the windward rail.

3, Only when the wheel raise on the windward side is higher than flange height could the wheelset derail out of the rail

4, With the breach becoming shorter, the flow passing through the breach speeds up, but the aerodynamic loads become weakened.

5, A critical overturning factor of 0.9 from the EN14067-6 [28] is more dangerous for the train, but that of the critical derailment coefficient from GB5599-85 [27] is safer with a large yaw moment. However, if the train is subjected to a large roll moment, the risk of overturning of the train may be higher than that of derailing. It is acceptable that the high-speed train passes by the windbreak breach with a distance less than 15 m at the speed of 120km/h, subjected to the normal wind speed of 32m/s.

7. Acknowledgement

This work was supported by Sichuan Science and Technology Program: [Grant Number 2019JDRC0131]; Doctoral Innovation Fund Program of Southwest Jiaotong University: [Grant

Number D-CX201816]; the National Natural Science Foundation of China: [Grant Number 51805451]; National Key R&D Program of China: [Grant Number. 2018YFB1201702], and a scholarship from the State Scholarship Fund of the China Scholarship Council.

References

1. Qiao Y, He D, Chen H, et al. Study on Aerodynamic Performance of Train Running in Wind Area. Journal of Dalian Jiaotong University. 2018;39(1):34-39.
2. Sun Z, Dai H, Gao H, et al. Dynamic performance of high-speed train passing windbreak breach under unsteady crosswind. Vehicle System Dynamics. 2019;57(3):408-424.
3. Wang D, Chen D, Li M, et al., editors. Research on aerodynamic characteristic for EMU passing by windbreak wall gap under crosswind. 2016 International Forum on Mechanical, Control and Automation (IFMCA 2016); 2017: Atlantis Press.
4. Liu D, Lu Z, Zhong M, et al. Measurements of car-body lateral vibration induced by high-speed trains negotiating complex terrain sections under strong wind conditions. Vehicle System Dynamics. 2018;56(2):173-189.
5. Liu D, Wang Q, Zhong M, et al. Effect of wind speed variation on the dynamics of a high-speed train. Vehicle System Dynamics. 2019;57(2):247-268.
6. Liu T, Chen Z, Zhou X, et al. A CFD analysis of the aerodynamics of a high-speed train passing through a windbreak transition under crosswind. Engineering Applications of Computational Fluid Mechanics. 2018;12(1):137-151.
7. Li T, Zhang J, Zhang W. Dynamic Performance of High-speed Train Passing Windbreak in Crosswind. Journal of the China Railway Society. 2012;34(07):30-35.
8. Miao X, Tian H, Gao G. The Influence of the Gorge Wind on the Aerodynamic Performance of the Train on Bridge. China Railway Science. 2010;31(6).
9. Miao X. Train Operation Safety under Transient Wind Load: Central South University; 2012.
10. Li P, Liang X, Niu J. Numerical simulation of the flow around a high-speed train moving through a crosswind flow. Journal of Railway Science and Engineering. 2017;14(6).
11. Baker C. A review of train aerodynamics Part 1–Fundamentals. The Aeronautical Journal. 2014;118(1201):201-228.
12. Baker C. A review of train aerodynamics Part 2–Applications. The Aeronautical Journal. 2014;118(1202):345-382.
13. Baker C. A framework for the consideration of the effects of crosswinds on trains. Journal of Wind Engineering Industrial Aerodynamics. 2013;123:130-142.
14. Baker C, Hemida H, Iwnicki S, et al. Integration of crosswind forces into train dynamic modelling. Proceedings of the Institution of Mechanical Engineers, Part F: Journal of Rail Rapid Transit. 2011;225(2):154-164.
15. Hemida H, Krajnović S. Exploring Flow Structures Around a Simplified ICE2 Train Subjected to A 30° Side Wind Using LES. Engineering Applications of Computational Fluid Mechanics. 2009;3(1):28-41.
16. Hemida H, Krajnovic S. Numerical study of the unsteady flow structures around train-shaped body subjected to side winds. European Conference on Computational Fluid Dynamics2006.
17. Hemida H, Krajnovic S, Davidson L, editors. Large-eddy simulation of the flow around a

simplified high speed train under the influence of a cross-wind. 17th AIAA Computational Fluid Dynamics Conference; 2005.

18. Hemida H, Krajnović S, Aerodynamics I. LES study of the influence of the nose shape and yaw angles on flow structures around trains. Journal of Wind Engineering. 2010;98(1):34-46.
19. Howell J. Aerodynamic response of maglev train models to a crosswind gust. Journal of Wind Engineering and Industrial Aerodynamics. 1986;22(2-3):205-213.
20. Kobayashi N, Yamada M. Stability of a one box type vehicle in a cross-wind-An analysis of transient aerodynamic forces and moments. SAE Technical Paper; 1988.
21. ANSYS I. ANSYS FLUENT Tutorial Guide ftp://ftp.energia.bme.hu/pub/Tuzelestechnika/MSc/flu_tg.pdf: ANSYS, Inc; 2010.
22. Zhou S, Zhang Z, Yang J. Simpack Example Tutorial (part 2). Beijing: Beijing united publishing company; 2013.
23. He D, Chen H, Yu W, et al. The influence of Wind wall on High-speed Train Aerodynamic Performance. Railway Locomotive &Car. 2016;36(5).
24. Sima M, Eichinger S, Blanco A, et al. Computational fluid dynamics simulation of rail vehicles in crosswind: Application in norms and standards. Proceedings of the Institution of Mechanical Engineers, Part F: Journal of Rail Rapid Transit. 2015;229(6):635-643.
25. Kang S O, Jun S O, Park H I, et al. Actively translating a rear diffuser device for the aerodynamic drag reduction of a passenger car [J]. International Journal of Automotive Technology, 2012, 13(4): 583-92.
26. Chen Z, Liu T, Jiang Z, et al. Comparative analysis of the effect of different nose lengths on train aerodynamic performance under crosswind [J]. Journal of Fluids and Structures, 2018, 78(69-85.
27. 5599-85 G. Railway vehicles-Specification for evaluation the dynamic performance and accreditation test. Bei Jing.
28. EN B. 14067-6, Railway applications--Aerodynamics Part 6: Requirements and test procedures for cross wind assessment. London: British Standard Institute.